THE TEMPORAL BOUNDARY LAYER UNDER THE ACTION OF DECAYING FREE-STREAM TURBULENCE

M. Kozul[1], R. J. Hearst[1], J. P. Monty[2], B. Ganapathisubramani[3] and D. Chung[2]

[1] Department of Energy and Process Engineering, NTNU, N-7491 Trondheim, Norway

[2] Department of Mechanical Engineering, University of Melbourne, VIC 3010, Australia

[3] Engineering and the Environment, University of Southampton, Highfield, Southampton SO17 1BJ, UK

melissa.kozul@ntnu.no

Abstract

The problem of the turbulent boundary layer under decaying free-stream turbulence is numerically investigated using the temporal boundary layer framework. This tool is particularly suited to the problem since the evolution of homogeneous isotropic turbulence is classically described by temporal decay. This study focuses on the interaction between the fully turbulent boundary layer and free-stream turbulence, which has so far received little attention compared to the behaviour of the transitional boundary layer subject to free-stream turbulence. The bulk of our simulations were completed by seeding the free-stream of boundary layers 'pre-grown' to a desired thickness with homogeneous isotropic turbulence from a precursor simulation. This strategy allowed us to test different combinations of the turbulence intensity and large-eddy lengthscale of the free-stream turbulence with respect to the velocity- and large-eddy length-scales of the boundary layer; such a parametric investigation would remain otherwise inaccessible given available computing resources. Additionally, the present strategy permits assessment of the direct effect of the locally present free-stream disturbances, as opposed to a 'downstream' effect from free-stream disturbances far 'upstream'. The relative large-eddy turnover timescale between the free-stream turbulence and the boundary layer emerges as an important parameter in predicting if the free-stream turbulence and boundary layer interaction will be 'strong' or 'weak' before the free-stream turbulence eventually fades away. For a 'strong' interaction, the main action of the free-stream turbulence on the boundary layer is to cause increased spreading of the boundary layer away from the wall, which then permits incursions of free-stream fluid deep within it, changing the boundary layer velocity profiles in the outer part of the flow. This has the important effect of increasing the boundary layer thickness δ by flattening the intermittency profile.

1 Introduction

Almost every boundary layer living in an engineering or environmental context is in fact exposed to free-stream disturbances. The present numerical study considers the interaction of free-stream turbulence (FST) with the fully turbulent temporal boundary layer to determine the conditions under which these free-stream disturbances are able to actively impart change upon the boundary layer.

A boundary layer developing under a free-stream laden with disturbances will tend to exhibit increased skin friction and mass or heat transfer (Blair, 1983a). Considerable effort (Hancock and Bradshaw, 1983; Blair, 1983b) has thus been made in the pursuit of formulating parameters able to correlate observed increases in skin friction coefficient C_f and mass (or heat) transfer coefficient St to parameters of the FST and the boundary layer. Such correlations are often based on a limited number of downstream locations in the experimental facility, whereas the current methodology is able to 'view' the entire interaction as it unfolds. The present simulations thus advance our understanding of the boundary layer-FST interaction via detailed DNS.

Recently, Kozul et al. (2016) demonstrated that the temporal boundary layer was a good model for the incompressible spatially developing turbulent boundary layer. Compared to the turbulent boundary layer with a quiescent free-stream, simulating this problem of a boundary layer with a turbulent free-stream is inherently more costly, since the free-stream with its disturbances must now also be adequately resolved. Employing a streamwise-shortened domain, the efficient temporal framework is well-suited to the current physical problem. Whilst wide-ranging scans of length-scales and intensities would be ideal to determine the true effect of each on their interaction with the boundary layer, in practice we are limited to cases where the free-stream lengthscale is a small multiple of the boundary layer thickness. The integral lengthscale of the FST must be much smaller than the domain size such that the associated large-scale energy-carrying eddies evolve freely (Thornber, 2016). A simulation with a free-stream lengthscale much larger than that of the boundary layer thickness is untenable given present computational capabilities - it would require the vast majority of the domain space, that is, available computational resources, to be dedicated to simulating the FST, when in fact our primary concern here is its

Case	Line	$Re_{\theta,0}$	$\frac{L^u_{e,0}}{\delta_0}$	$\frac{u'_{e,0}}{U_w}(\%)$	$\frac{u'_{e,0}}{u_{\tau,0}}$	$\frac{T_{\delta,0}}{T_{e,0}}$
A	——	47	19	4.9	-	-
A1	——	508	1.7	3.7	0.71	0.38
B	——	508	3.2	5.0	1.0	0.28
C	——	1413	0.54	10	2.3	3.7
D	——	506	1.6	10	1.9	1.1
E	——	720	1.1	10	2.1	1.7

Table 1: Parameters of the present simulations of boundary layers developing under decaying FST. Different values of $(L^u_e/\delta)_0$ are achieved by introducing the HIT into the free-stream of a temporal boundary layer developing in a quiescent field at various $Re_\theta = U_w\theta/\nu$, with momentum thickness θ, or equivalently, times t_0. $T_\delta = \delta/u_\tau$ is the boundary layer large-eddy turnover timescale. Note the large difference in $T_{\delta,0}/T_{e,0}$ between cases C and D: the only difference is that the boundary layer was 'pre-grown' to a higher Reynolds number in case C before the FST was added. The boundary layer thus has a much larger large-eddy turnover timescale than case D, or the FST.

interaction with the boundary layer. In fact, the response of the boundary layer to small-scale turbulence in the free-stream remains rather under-explored compared to that of large-scale FST (Nagata et al., 2011).

Since many engineering problems feature turbulent boundary layers exposed to ambient free-stream conditions that cannot realistically be considered laminar, our work illustrates when and how such free-stream disturbances affect heat and mass transfer via active manipulation of the boundary layers forming over walls.

2   Simulation setup

Hereafter, we will refer to fluctuating velocities u, v and w in the x- (streamwise), y- (spanwise) and z- (wall-normal) directions. The appropriate Reynolds decomposition for the temporally developing turbulent boundary layer is given by $u_i = \overline{u}(z,t)\delta_{i1} + u'_i(x,y,z,t)$, where $\overline{(\cdot)}$ indicates averaging in the homogeneous xy-planes. The previously quiescent free-stream of the turbulent temporal boundary layer is now seeded with homogeneous isotropic turbulence (HIT) generated in a triply periodic domain in a precursor simulation using the spectral code of Chung and Matheou (2012). Quantities external to the boundary layer will be identified with subscript e, and values at the beginning of the combined simulations with subscript 0. The FST-boundary layer cases will be characterised by a free-stream turbulence intensity u'_e/u_τ, for friction velocity u_τ, and a large-eddy lengthscale ratio L^u_e/δ, for 99% boundary layer thickness $\delta \equiv \delta_{99}$. L^u_e was defined by Hancock and Bradshaw (1983) as:

$$U_e\frac{\mathrm{d}(\overline{u'^2})_e}{\mathrm{d}X} = \frac{-(\overline{u'^2})_e^{3/2}}{L^u_e}, \qquad (1)$$

for mean streamwise free-stream velocity U_e and distance from the turbulence-producing grid X. This is of course not the only manner in which to define the energy-carrying integral lengthscale of the FST. A common definition has been the first zero crossing of the integrated normalised autocorrelation. However this quantity is problematic because this zero-crossing is somewhat elusive (Dogan et al, 2016); a dissipation-based scale is much better-defined. For perfectly isotropic turbulence, this lengthscale can be written as

$$L^u_e = \frac{3}{2}\frac{(\overline{u'^2})_e^{3/2}}{\epsilon}, \qquad (2)$$

for kinetic energy dissipation rate $\epsilon \equiv \nu\overline{(\partial u'_i/\partial x_j)^2} = 15\nu\overline{(\partial u'/\partial x)^2}$ in HIT (Hinze, 1959) with kinematic viscosity ν. A desired $(L^u_e)_0$ in the FST was achieved via forcing to a selected shell of wavenumbers centred on forcing wavenumber k_f. From preliminary simulations we have established

$$k_f(L^u_e)_0 \approx 5, \qquad (3)$$

with a thin forcing shell thickness ($\Delta k\,\eta_0 = 0.0072$, where η_0 is the Kolmogorov lengthscale at the beginning of the combined simulation). The range of relative length- (L^u_e/δ) and velocity- (u'_e/u_τ) scale ratios was extended by injecting the HIT into the free-stream of boundary layers that had been 'pre-grown' to different thicknesses δ or equivalently, Reynolds numbers. The HIT decays according to established power laws and care was taken to ensure that the domain size did not constrict this decay. Kozul (2018) provides more details about the HIT simulations. At the moment of injection into the free-stream, the Taylor Reynolds number is $Re_{\lambda,0} = u'_{e,0}\lambda_{e,0}/\nu \approx 82$, for Taylor microscale λ, for all cases except A1 in table 1, for which it is $Re_{\lambda,0} \approx 52$. Forcing to the HIT is removed at the moment of injection into the boundary layer's free-stream. That is, the HIT fields begin to decay at the moment when the combined simulation with synthesised initial conditions is launched. Case A1 is a companion simulation to case A, where the HIT for case A1 is that for case A (and all others) but allowed to decay within the precursor HIT simulation before injection for the same interval of time as needed by case A to reach $Re_\theta \approx 500$. This was done such that we could investigate the 'recovery' time required following the artificial combination of the fields. Despite being modest, the present Taylor Reynolds numbers for the HIT still admit power-law decay of the kinetic energy as predicted by theory. A time interval $\Delta t/T_{e,0} \approx 1$ is required before the u'_e of the HIT begins this power law decay.

The finite-difference code used for both the 'pre-grown' boundary layers and the synthesised fields for which statistics are presented herein has been validated in Chung et al. (2014). The fields are combined via thresholding on the passive scalar c that is released at the wall and also solved for in the precursor simulations of the boundary layer; it was thought that this would lead to a smaller bias toward any one component of velocity. The HIT is first interpolated using cubic splines onto the stretched grid required by the temporal boundary layer simulation. A function effectively masking the HIT by the boundary layer then gives a combined field $\underline{u}_0 = \alpha \underline{u}_{HIT} + (1 - \alpha)\underline{u}_{BL}$ with

$$\alpha(\underline{x}) = \begin{cases} 0, & 0 \leq \frac{c - C_w}{C_\infty - C_w} \leq 0.95 \\ 1, & 0.95 < \frac{c - C_w}{C_\infty - C_w} \leq 1, \end{cases} \quad (4)$$

for $\underline{x} = (x, y, z)$ and $\underline{u} = (u, v, w)$, as shown in figure 1. $C_w - C_\infty$ is the difference between the boundary scalar values at the bottom wall and free-stream. All cases except case A are formed thus; for case A the HIT fields form the entire initial field. No HIT fluctuations were added to the scalar field. Physical quantities for the present cases are given in table 1.

Periodic boundary conditions are imposed in the streamwise direction x as well as the spanwise direction y. A 'conveyor-belt' moving-wall setup is used. At this bottom wall where $z = 0$, $u = U_w$ and $v = w = 0$ are imposed. The top boundary ($z = L_z$) is a fixed wall with an impermeable ($w = 0$) boundary condition, and slip boundary conditions on the velocities tangential to the wall ($\partial u/\partial z = \partial v/\partial z = 0$). The usual configuration, with a stationary no-slip wall and non-zero free-stream velocity U_∞, is recovered via Galilean transformation. An initial trip $Re_D \equiv DU_w/\nu \approx 500$ is used to trigger transition of the precursor boundary layer simulations to a turbulent regime as in Kozul et al. (2016). The pressure gradient is set to zero. We used a domain where $L_x = 2 L_y = 2 L_z$. The simulations can be run until one of the box constraints are met: either $L_e^u \approx L_z/10$, or $\delta \approx L_z/3$.

3 Results

Figure 2 shows streamwise velocity fields overlaid with vorticity magnitude contours at two times for case D. Figure 2(a) is at the moment when the free-stream is seeded with HIT, where vorticity contours are drawn only for the boundary layer (before FST injection) for clarity. The strong velocity fluctuations in the free-stream have faded significantly in figure 2(b) at a later time. Figure 3 places our simulations amongst several previous experimental studies. The current cases begin at the top right of each of the curves and track downwards and to the left in time as do those of Hancock and Bradshaw (1983) as the measurements move downstream in their wind tunnel. The curve for case
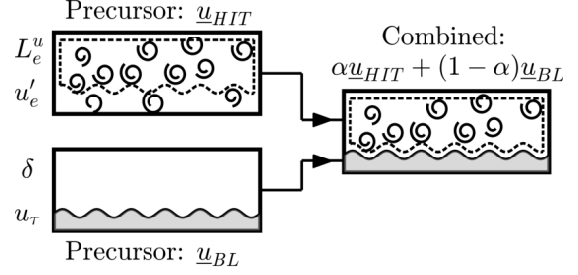

Figure 1: Schematic of the combined fields formed from precursor simulations via masking (4) using the scalar concentration of the boundary layer, represented by the grey shaded area. BL = boundary layer, HIT = homogeneous isotropic turbulence.
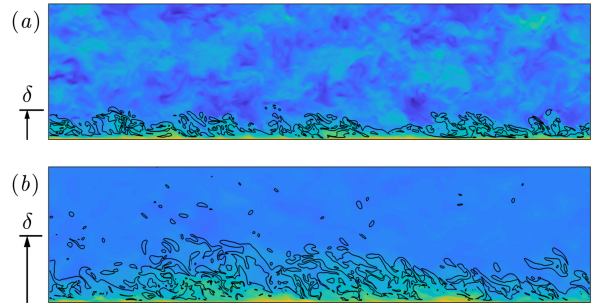

Figure 2: Indicative streamwise velocity field overlaid with contours of vorticity for case D: (a) $\Delta t = 0$, at the moment when the FST is injected into the free-stream; (b) $\Delta t \approx 3.8\ T_{e,0}$ after FST injection. Vorticity contours in (a) are those of the boundary layer before FST injection, showing its 'pre-grown' extent. Black contour lines are drawn at $|\omega| = 1.4\ U_w/\delta$. Actual vertical extent of the domain is twice that shown. The wall moves to the right.

A (HIT fields form initial simulation fields) is only plotted from $Re_\theta \approx 500$ onwards such that the growing boundary layer is behaving canonically following bypass transition. Most of the present cases demonstrated the oft-cited increase in both skin friction coefficient C_f and mass transfer coefficient or Stanton number St. However, we found the observed increase was due in large part to the enhanced development rate of the boundary layer thickness δ at fixed $\Delta Re_{X=U_w t}$ post-HIT injection, rather than a change of the streamwise velocity gradient at the wall. Since C_f canonically decreases with increasing Reynolds number, artificially increasing, say, $Re_\tau = \delta u_\tau/\nu$ via an increase in δ will register as a gain in C_f over the canonical value for that new increased Reynolds number. This is to be expected given that the FST is an outer-flow effect by design in our simulations, but draws attention nonetheless to the fact that a shift in Reynolds number can cause an apparent increase in C_f over that for a canonical boundary layer with a quiescent free-stream.

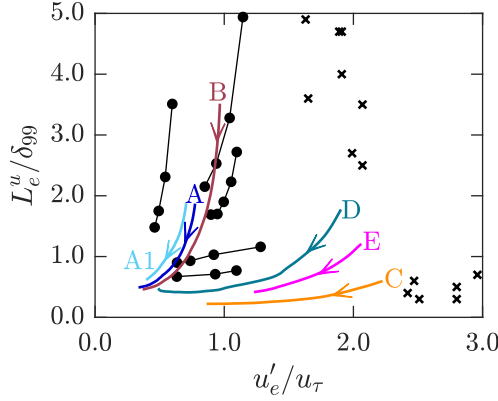Notwithstanding a non-physical adjustment period

Figure 3: Regime diagram showing completed cases (coloured curves as per table 1); ●, Hancock and Bradshaw (1983); ×, Dogan et al. (2016). Connected curves track downwards toward the left-bottom corner.

after the artificial combination of fields, we are able to find some agreement with an experimental study of the same problem (Nagata et al, 2011) for case D in figure 4, which shows subdued mean streamwise velocity and w_{rms}^+ profiles. The small-scale turbulence of Nagata et al. (2011) allows for qualitative comparison to the present cases, although the upstream history is different compared to our synthesised fields. Re_τ and u_e'/u_τ are matched, although the lengthscale ratio L_e^u/δ differs. Yet in both cases this ratio is well under 1. The profile of u_{rms}^+ (not shown) is identical to the quiescent case at matched Re_τ from the wall up to $z^+ \approx 400$. Although we would not necessarily expect to find agreement with this experimental boundary layer, which has been exposed to FST from inception in contrast to ours, for our case D the FST has effected change deep into the boundary layer. An important change is the reduction of the wake in the outer region in the mean streamwise profile in figure 4(a): Blair (1983b) reported that the wake is totally subdued for a value of around $u_e'/U_\infty \approx 0.05$. For this level of turbulence at $u_e'/u_\tau = 0.50$, $u_e'/U_w \approx 0.02$, we find the wake weakened yet still present. The diminishing wake is a manifestation of diminishing intermittency in the outer region of the boundary layer due to the free-stream disturbances. Our injected FST therefore impacts our boundary layer in a similar way to this particular experimental case. Thus we consider this an example of a 'strong' boundary layer-FST interaction. In contrast to these modified profiles for case D, similar profiles for case C showed no change from the quiescent profiles due to the presence of the FST. We highlight here that there is a large difference in $T_{\delta,0}/T_{e,0}$ between cases C and D, which may explain why the boundary layer in case C appears to ignore the FST in an apparent 'weak' interaction with it.

The intermittency factor γ is shown in figure 5 for cases C and D. It is here calculated as the percentage of points in a homogeneous xy-plane that are

above a certain threshold value of the scalar c, to compare against the intermittency profiles offered in Hancock and Bradshaw (1989), where it was defined as the fraction of total time for which the flow at the measured position is 'hot' in their heated boundary layer. A thresholding value of 1% of the scalar contrast $C_w - C_\infty$ was used such that curves in 5(a), when the FST velocity fields are injected, resembled those of Hancock and Bradshaw (1989) for their $u_e' = 0$ case. Figure 5(b) shows the profiles of γ at $\Delta t \sim 0.9\, T_{e,0}$ after insertion of the FST, that is, after roughly one eddy-turnover time of the FST. We find that the effect of the FST is to spread the boundary layer edge, more so for case D, yet not insignificantly for case C.
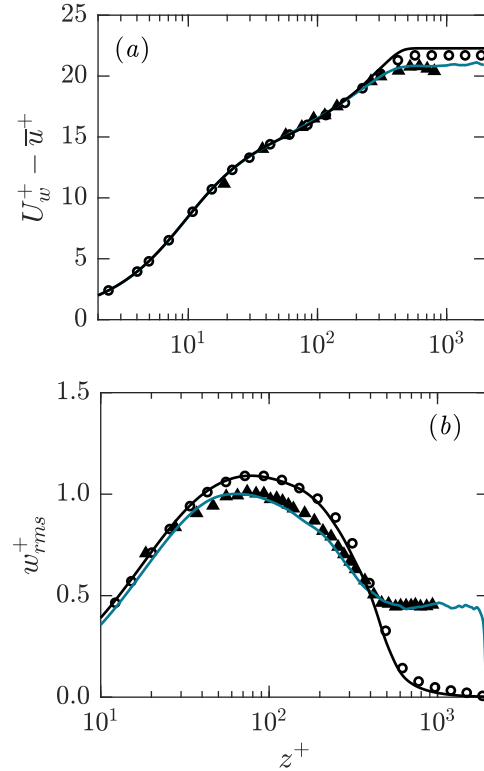

Figure 4: Altered profiles for case D at $Re_\tau \approx 450$: (a) mean streamwise velocity; (b) root-mean-squared wall-normal velocity fluctuations; ——, quiescent temporal boundary layer from Kozul et al. (2016) at matched Re_τ; ——, present simulation case D ($L_e^u/\delta = 0.403$, $u_e'/u_\tau = 0.43$); ○, quiescent spatial boundary layer of Simens et al. (2009) at $Re_\tau = 445$; ▲, experimental case LG-2 of Nagata et al. (2011) at $Re_\tau = 475$ ($L_e^u/\delta = 0.235$, $u_e'/u_\tau = 0.45$).

4   Free-stream contributions to mean profiles

Figure 6 shows the 'free-stream' vs. 'boundary layer' contributions to the wall-normal Reynolds stress profile $\overline{w'^2}/u_\tau^2$ for the present cases C and D. We here use the same thresholding for the conditional averages as was used for the injection of the FST itself: if the
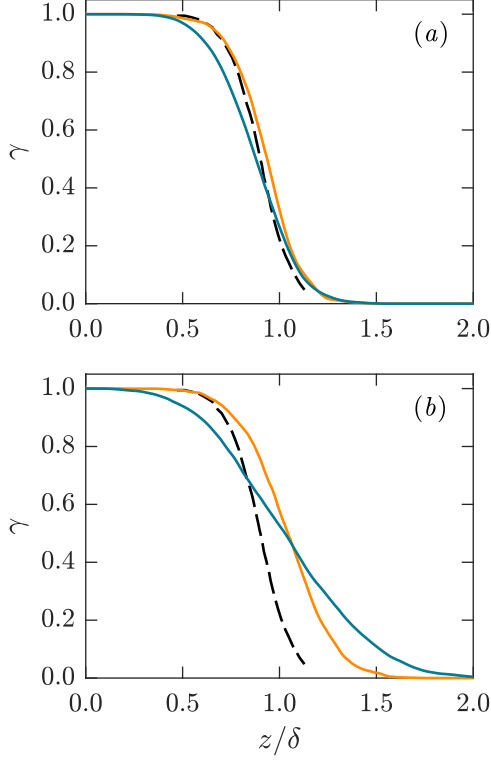
Figure 5: Intermittency factor: calculated as the fraction of points at each homogeneous xy-plane where the scalar exceeds 1% of $C_w - C_\infty$, the scalar contrast; (a) $Tu_e \equiv u'_e/U_w \approx 10\%$ at FST injection; (b) $Tu_e \approx 5.7\%$ at a later time after $\Delta t \sim 0.9\,T_{e,0}$; $---$, line of Hancock and Bradshaw (1989) for $u'_e = 0$; ——, case C ('weak' interaction); ——, case D ('strong' interaction).

scalar concentration is below 5% of the scalar wall contrast $C_w - C_\infty$, it will be considered to be a free-stream contribution, else it is deemed to have originated in the boundary layer for the purposes of the present analysis. This was confirmed to differ from similar profiles for the baseline case of the quiescent boundary layer. At the time of FST injection (figures 6a and 6b) the profiles, and especially, the FST contributions, appear similar for the two cases. However the picture changes at a later time. For figures 6(c) and 6(d), after about $\Delta t \sim 0.9\,T_{e,0}$, the same delay considered in the intermittency profiles in figure 5 (and roughly the same intervals in terms of FST large-eddy timescale $T_{e,0}$ for each case), the contribution to the total profile by 'free-stream' fluid is almost zero below $z/\delta \approx 0.4$ for case C. Yet for case D there is a significant incursion of 'free-stream' fluid all the way through the boundary layer. This is despite a smaller relative lengthscale L_e^u/δ. Our curves, especially for case D, show remarkable qualitative similarity with those of Hancock and Bradshaw (1989) at the later time, which helps to bolster confidence in the ability of our artificially-synthesised fields to replicate not only mean statistics of laboratory fields, but also the rela-

tive contributions of the free-stream and the boundary layer. As they stated, we too see a substantially altered structure in the outer layer, while the main effect in the inner layer is increased 'inactive' motions from the free-stream.

The straight-line attenuation of the free-stream contribution is striking in figure 6(c) for case D at $L_e^u/\delta = 0.52$, having been concave at the time of injection in figure 6(a). This is a demonstration of the attenuation of the wall-normal component of velocity due to the wall-blocking effect, that is, the normal-component velocity constraint at the wall (Hancock and Bradshaw, 1989). This explains the more rapid increase in similar curves for $\overline{u'^2}/u_\tau^2$ than for $\overline{w'^2}/u_\tau^2$ as we move away from the wall. In contrast, the free-stream contribution for case C in figure 6(d) after a time delay remains rather curved as it is at FST injection in 6(b), pointing to different adjustment times of the boundary layers to the FST. The 'inactive' motion intrusions into the boundary layer in this case cause a decrease in the wall-normal variance for case D as was seen in figure 4(b).

Hancock and Bradshaw (1989) found conditionally sampled statistics showed a dependence on $e = (u'_e/L_e^u)/(u_\tau/\delta) = T_\delta/T_e$, which they identified as a relative fluctuating strain. However they found that at large e, statistics were no longer dependent on this parameter. Whilst this implies that the FST has a large relative fluctuating strain compared to the boundary layer, making this, as they noted, 'unexpected', identifying it here as a relative timescale, we offer the explanation that a large e means that the FST will decay rather more rapidly than the boundary layer is apparently able to adjust to or absorb its effects.

5   Conclusions

In conducting simulations of boundary layers exposed to FST, we found examples of both 'strong' interactions (case D), and 'weak' interactions (case C), where there was no significant change in C_f development, or any modification of velocity profiles from the case with a quiescent free-stream. This is despite reasonably high FST intensities u'_e/u_τ. Flattened intermittency profiles were observed for both cases, suggesting that whilst the boundary layer in case C ('weak' interaction) is indeed susceptible to change via the action of the FST, the FST decays more rapidly than the rate at which the boundary layer is able to absorb changes in its velocity profiles. That is, the strength, or effect of, the interaction cannot be solely predicted from knowledge of the relative large-eddy lengthscale ratio L_e^u/δ or free-stream intensity in isolation, as suggested from the summary of experimental results of this problem presented in Nagata et al. (2011). A flattened intermittency profile is indicative of an increased 99% boundary layer thickness, which can have the effect of causing an apparent increase in skin friction coefficient C_f for a given Re_τ; for most
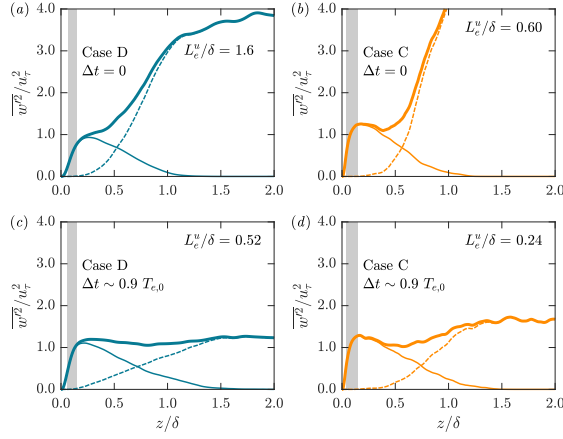
Figure 6: Boundary layer and FST contributions to the wall-normal Reynolds stress profile: ———, contribution from the boundary layer; − − −, contribution of FST; ▬▬, sum of two profiles, equivalent to conventionally-averaged profiles. (*a*) and (*c*), case D; (*b*) and (*d*), case C. Figures (*a*) and (*b*) are at the time of FST injection, figures (*c*) and (*d*) are after $\Delta t \sim 0.9\, T_{e,0}$. Grey shaded region spans the logarithmic region $3Re_\tau^{1/2} < z^+ < 0.15Re_\tau$ as suggested by Marusic et al. (2013).

of our cases, this gain in C_f over the canonical value is due to this increase in friction Reynolds number provoked by the FST for the monotonically-decreasing C_f profile, rather than a genuine change in the mean streamwise velocity gradient (and therefore u_τ) at the wall. We were able to discern free-stream vs. boundary layer contributions to the wall-normal Reynolds stress profile by conditioning Reynolds stress statistics on the scalar released at the wall. We found that the boundary layer in case C ('weak' interaction) was indeed receiving contributions from the FST, but that they did not penetrate deeply as quickly in time as those for case D ('strong' interaction).

A consistent explanation for this effect appears to be a difference in relative large-eddy timescale $T_{\delta,0}/T_{e,0} = e_0 = (\delta/u_\tau)_0/(L_e^u/u_e')_0$ at FST injection: this quantity differed by a factor of 3 for the two cases C and D we focused on in this paper. If $e \lesssim 1$, meaning the FST has time to 'strongly' interact with the boundary layer, the main action of the FST is to cause increased spreading away from the wall, with the important effect of increasing the growth rate of the boundary layer thickness δ, which then permits incursions of free-stream fluid deep within it. This gives rms velocity profiles that appear as an average of the FST and canonical boundary layer values. On the other hand, $e \gtrsim 1$ in the present cases resulted in 'weak' interactions, where the boundary layer was unable to 'see' the FST before it faded away. The ability of the FST to change the boundary layer requires the boundary layer to have time - measured in its *own* time - to react to it.

References

Blair, M. F. (1983), Influence of Free-Stream Turbulence on Turbulent Boundary Layer Heat Transfer and Mean Profile Development, Part I - Experimental Data, *Trans. ASME: J. Heat Transfer*, Vol. 105, pp. 33-40.

Blair, M. F. (1983), Influence of Free-Stream Turbulence on Turbulent Boundary Layer Heat Transfer and Mean Profile Development, Part II - Analysis of Results, *Trans. ASME: J. Heat Transfer*, Vol. 105, pp. 41-47.

Chung, D. and Matheou, G. (2012), Direct numerical simulation of stationary homogeneous stratified sheared turbulence, *J. Fluid Mech.*, Vol. 696, pp. 434-467.

Chung, D., Monty, J. P. and Ooi, A. (2014), An idealised assessment of Townsend's outer-layer similarity hypothesis for wall turbulence, *J. Fluid Mech.*, Vol. 742, R3.

Dogan, E., Hanson, R. E. and Ganapathisubramani, B. (2016), Interactions of large-scale free-stream turbulence with turbulent boundary layers, *J. Fluid Mech.*, Vol. 802, pp. 79-107.

Hancock, P. E. and Bradshaw, P. (1983), The effect of free-stream turbulence on turbulent boundary layers, *Trans. ASME I: J. Fluids Engng*, Vol. 105, pp. 284-289.

Hancock, P. E. and Bradshaw, P. (1989), Turbulence structure of a boundary layer beneath a turbulent free stream, *J. Fluid Mech.*, Vol. 205, pp. 45-76.

Hinze, J. (1959), Turbulence: An Introduction to its Mechanisms and Theory, *McGraw-Hill*.

Kozul, M.,Chung, D. and Monty, J. P. (2016), Direct numerical simulation of the incompressible temporally developing turbulent boundary layer, *J. Fluid Mech.*, Vol. 796, pp. 437-472.

Kozul, M. (2018), The turbulent boundary layer studied using novel numerical frameworks, *PhD Thesis, University of Melbourne*.

Marusic, I. and Monty, J. P. and Hultmark, M. and Smits, A. J. (2013), On the logarithmic region in wall turbulence, *J. Fluid Mech.*, Vol. 716, R3.

Nagata, K., Sakai, Y. and Komori, S. (2011), Effects of small-scale freestream turbulence on turbulent boundary layers with and without thermal convection, *Phys. Fluids*, Vol. 23, 065111.

Thornber, B. (2016), Impact of domain size and statistical errors in simulations of homogeneous decaying turbulence and the Richtmyer-Meshkov instability, *Phys. Fluids*, Vol. 28, 045106.

Simens, M. P., Jiménez, J., Hoyas, S. and Mizuno, Y. (2009), A high-resolution code for turbulent boundary layers, *J. Comput. Phys.*, Vol. 228, pp. 4218–4231.